



This is a preview version of our white paper on surface treatment by ion implantation

To get the full version, just send us an e-mail: **info@idonus.com**

WHITE PAPER

Surface treatment by ion implantation

Case study: Nitrogen implantation in brass as an efficient means to lower the coefficient of friction and improve the wear resistance of miniature parts

Ion implantation equipment and surface treatment

idonus sàrl, Hauterive, Switzerland

Dr. Christophe YAMAHATA, *Project Manager*

Thomas WATTENHOFER, *Automation Engineer*

Christian SPOERL, *Managing Director*

Tribological characterization and material analysis

CSEM SA, Neuchâtel, Switzerland

Materials Science and Component Reliability

Dr. Kaushik VAIDEESWARAN

Silvia BISELLI

Dr. Massoud DADRAS

Ion implantation can be applied to a wide variety of materials to enhance their surface properties (*e.g.*, stainless steel, titanium, sapphire, silicon, rubber, PEEK).

This white paper showcases some benefits of this technology through a thorough tribological study of machinable brass implanted with nitrogen ions.

The document is divided into two parts that can be read independently:

I. **Technology** (pp. 2–5)

Introduction to ion implantation technology and equipment used for surface treatment

II. **Case study** (pp. 6–14)

Multi-charged nitrogen ion implantation in machinable brass

In the case study devoted to brass alloy CuZn39Pb3, we demonstrate the lowering of the coefficient of friction from 0.7 to 0.25 (system: brass vs. quenched steel) as a result of nitrogen ion implantation. Surface wear of brass could be drastically reduced, even with a contact pressure in the range of 300 MPa.



ION IMPLANTATION is the principal technology used to introduce foreign elements into solids in a uniform and controlled way. The technology was initially developed by the semiconductor industry for the doping of materials. It is now being increasingly adopted for the surface treatment of a variety of materials. Before getting into this topic, we shall take a brief look at the history of ion implantation.

Semiconductor doping and surface engineering

In semiconductor terminology, doping refers to the fabrication process in which impurity atoms are intentionally introduced in the exposed area of a semiconductor for the purpose of modifying its electrical characteristics. Shockley¹ was the first to foresee the potential of ion implantation for the doping of semiconductor wafers, as evidenced by his 1954 patent application entitled “Forming semiconductive devices by ionic bombardment” [1]. However, it was only in the late 1970s that ion implanters entered the industry of semiconductors. Since then, ion implantation has been the principal doping method used for integrated circuits (IC) manufacturing [2].

The technology involves the generation of an ion beam and steering it in a controlled manner. Ionized species are accelerated by electric fields to high energies and shot into a target substrate. They can also be separated by magnetic fields to obtain an ion beam of high purity and a well-defined energy. Research in particle physics shares the same needs in terms of high purity ion beam handling and has played an essential role in the rise of ion implantation. Key technologies have emerged from the efforts made in building efficient ion sources and high-energy particle accelerators, not to mention the hardware required to generate high-power

their researches on semiconductors and their discovery of the transistor effect.”

¹ William Bradford Shockley, John Bardeen and Walter Houser Brattain were jointly awarded the Nobel Prize in Physics 1956 “for

radio-frequency (RF) electromagnetic waves and high-voltage DC (direct current) electric fields.

A major reason in applying ion implantation for doping semiconductors lies in that critical process parameters, such as amount and position of implanted species (concentration and penetration depth), are equipment settings directly controlled by the dose and energy, respectively. To fulfil the many implantation applications found in ICs, the doping requirements span several orders of magnitudes in both dose (10^{11} to 10^{17} atoms/cm²) and energy levels (100 eV to nearly 10 MeV), for a wide range of atomic species (P, B, As, In, Ge, N, H, He, etc.).

Besides technological advances, studies were also undertaken to better understand ion stopping and thus address the needs for accurate doping. Theoreticians have refined models describing collision of ions with matter. On this topic, much is owed to Ziegler *et al.* who have developed SRIM, a Monte Carlo computational algorithm whose acronym stands for "Stopping and Range of Ions in Matter" [3]. SRIM was released as a freeware and is currently the most widely used tool by the scientific community to simulate the interaction of accelerated ions with matter [4]. It is primarily used to determine the penetration depth and distribution of atoms (projected range and straggling) based on the energy of ions and their angle of incidence with respect to a target material.

We now leave aside the field of semiconductors to focus on the needs that are specific to surface treatment. Noticeable changes in material surface properties can be obtained for doses in the range of 10^{15} to 10^{18} atoms/cm² and for energies between tens to few hundred keV. Literature survey shows that a number of atomic species have been implanted, often extracted from gaseous elements (N, O, H, He, C, Ar, etc.), but also from solid-state materials, mainly to produce metallic ion beams (Cu, Au, Ag, etc.). Owing to its ease of production and handling – and its many proven effects – nitrogen is the foremost species used for surface treatment by ion implantation.

In light of the requirements mentioned above, the primary specification for a surface treatment implanter is to produce large ion beam currents to ensure cost effectiveness of the process for high-dose applications. Indeed, the greater the beam current, the faster the implantation. However, but not surprisingly, many

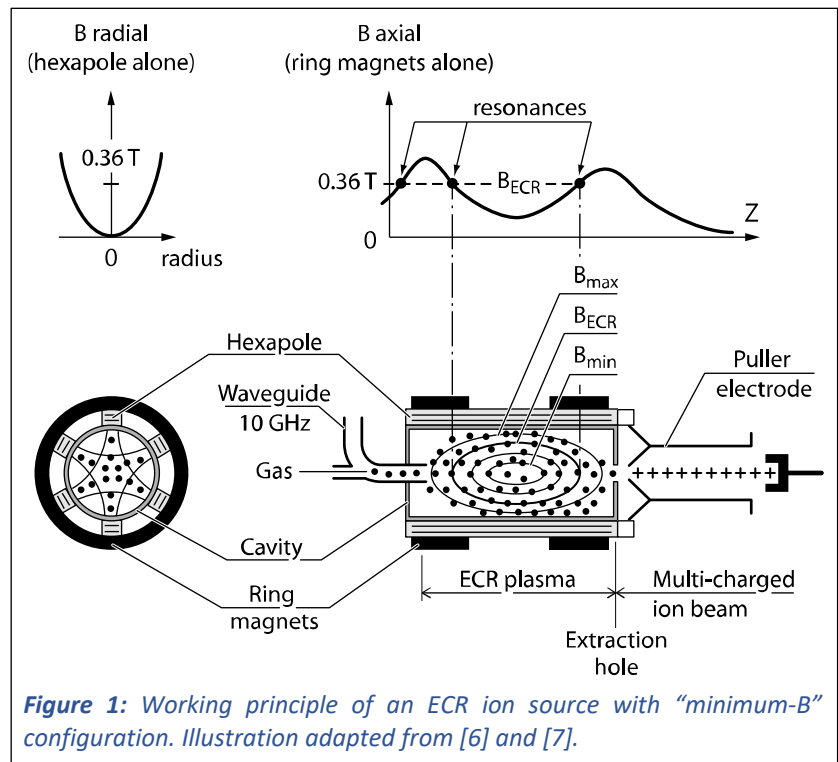


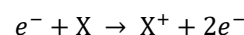
Figure 1: Working principle of an ECR ion source with "minimum-B" configuration. Illustration adapted from [6] and [7].

surface treatment studies have been carried out with implanters dedicated to semiconductor wafers or using in-house modified versions of these facilities. Clearly, the demands for semiconductor implantation are different from those for surface engineering. The same applies to the ion source: While high purity and precise dose control are critical parameters for IC doping, throughput is the primary criterion for surface treatment.

Electron Cyclotron Resonance (ECR) ion source

Among the wide variety of ion sources that have been invented, the ECR ion source has several great characteristics that makes it particularly suited for surface treatment. It produces positive ions with charge states reaching unparalleled levels [5]. The ECR ion source was pioneered in the 1970s by Richard Geller at the CEA² [6, 7]. It is now widely used in accelerator physics and can be found in leading-edge research facilities such as the Linear Accelerator 3 (LINAC 3) at CERN³. We shall first present its operating principle (see Figure 1), since it will prove useful for the understanding of the process discussed below.

Gas discharge – The ECR ion source uses a gas discharge plasma to create positive ions. A gas discharge plasma is an ionized gas sustained by applying an electric field across it. Positive ions are created by electrons that supply the dissociative ionization energy when they collide against atoms. The basic gas phase reaction is



² French Alternative Energies and Atomic Energy Commission or CEA (Commissariat à l'Énergie Atomique).

³ European Organization for Nuclear Research, known as CERN.

Case study: Ion implantation of nitrogen in machinable brass

Abstract — We investigate the tribological effects of multi-charged ion implantation (MCII) of nitrogen in CuZn39Pb3 alloy, a machinable brass that is widely used in the watchmaking industry. For this study, MCII of nitrogen was performed at 35 kV with a fluence of 5×10^{17} atoms/cm² and has resulted in a threefold decrease of the coefficient of friction (COF), from 0.7 to 0.25, as measured with a ball-on-disc tribometer. Wear track profile measurements using Atomic Force Microscopy (AFM) on the tribological traces showed that the wear rate was lowered by two orders of magnitude, from 10^{-14} m²/N for the untreated reference to 2.9×10^{-16} m²/N for the implanted brass. Implanted samples were observed by transmission electron microscopy (TEM) and the results corroborate well with Monte Carlo simulations. Further analyses with Energy-Dispersive X-Ray Spectroscopy (EDS) and Grazing Incidence X-Ray Diffraction (GIXRD) showed that nitrogen implantation in brass did not result in the formation of a new crystalline phase. Hence, the enhanced tribological properties of brass could be attributed to the modification of surface microstructure of brass following high energy ion implantation.

Introduction

Ion implantation is well known for significantly modifying the mechanical, electrical, optical, and chemical properties of all categories of solid materials (metals, polymers, ceramics, semiconductors, composites). The primary use of ion implantation is in semiconductor doping, but several other industrial applications have started to emerge [13]. For instance, structural rearrangement in optical materials causes changes in the refractive index. Ion implantation can hence be used as an anti-reflective treatment, or to produce waveguides. Advanced applications based on ion implantation technology are also being developed for catalysis systems, and more generally for chemical surface functionalization, or for biocompatibility enhancement. Finally, the potential for mechanical applications is vast and this field is probably the one that is currently undergoing the strongest developments. In this study, we will discuss the tribological properties of brass that can be improved by ion implantation.

When compared with other surface treatments, ion implantation has several unique advantages:

- Dimensional changes are insignificant, or restricted to the atomic level;
- Solid solubility limit can be exceeded;
- Depth distribution is controllable;
- As its name implies, particles diffuse into the matter, thus eliminating delamination risks;
- The process can be completed at low temperature.

These characteristics are sought after in fine mechanics. Of course, like other processes, the technology also has some limitations. One being that ion beam implantation is a line-of-sight treatment. Re-entrant surfaces cannot be treated effectively. Nevertheless, this issue can be tackled if the functional areas can be scanned under the ion beam using an adapted sample stage. The technology is thus particularly attractive for miniature mechanical parts, like those found in high-end watches.

The tribological effects of ion implantation have been largely studied and the proven improvements include: surface hardening, low friction, increased wear resistance, and improved corrosion reduction. One or several of these effects have been demonstrated in a wide variety of materials: plastics (*e.g.*, PEEK, PMMA, PC) and elastomers (*e.g.*, NBR, EPDM, FKM rubbers), brittle materials (such as silicon, glass, sapphire, ceramics), and of course metals. Ion implantation in metallic alloys has been investigated in detail (especially in steels [14, 15, 16], but also in aluminium alloys [17, 18], and in titanium alloys [19]). Yet, only few studies have been devoted to ion implantation in brass or copper.

In a research report dating from 1985, Shih showed that nitrogen implantation had a positive effect on impact wear for various metals (100 keV, dose of about 4×10^{17} atoms/cm²) [20]. For unexplained reasons, it did not prove successful on cartridge brass (70 wt % Cu / 30 wt % Zn), but the results were significant on copper, bronze (90 wt % Cu / 10 wt % Sn), aluminium alloys and 304 stainless steel, among other tested metals. Improvement in impact wear resistance was attributed to the hardening effects of nitrogen implantation. These effects could be explained either in terms of interstitial hardening, or by the formation of very hard nitride phases, or by a combination of both processes. These two strengthening processes act by impeding the movement of dislocations. The first one involves the segregation of interstitial nitrogen atoms at the core of dislocations [21]. More recently, Sari *et al.* showed surface hardening as well as increased corrosion resistance of Cu (99% purity) after nitrogen implantation (50 keV, fluence of 3×10^{17} atoms/cm²) [22]. A recent work by Zharkov *et al.* showed wear reduction of copper samples implanted with nitrogen (20 keV, fluence of 9×10^{17} atoms/cm²) caused by surface hardening [23]. They attributed hardening in copper to the refinement of the grain structure (nanostructuring) of the main FCC-Cu phase (face-centred cubic structure) occurring at high-

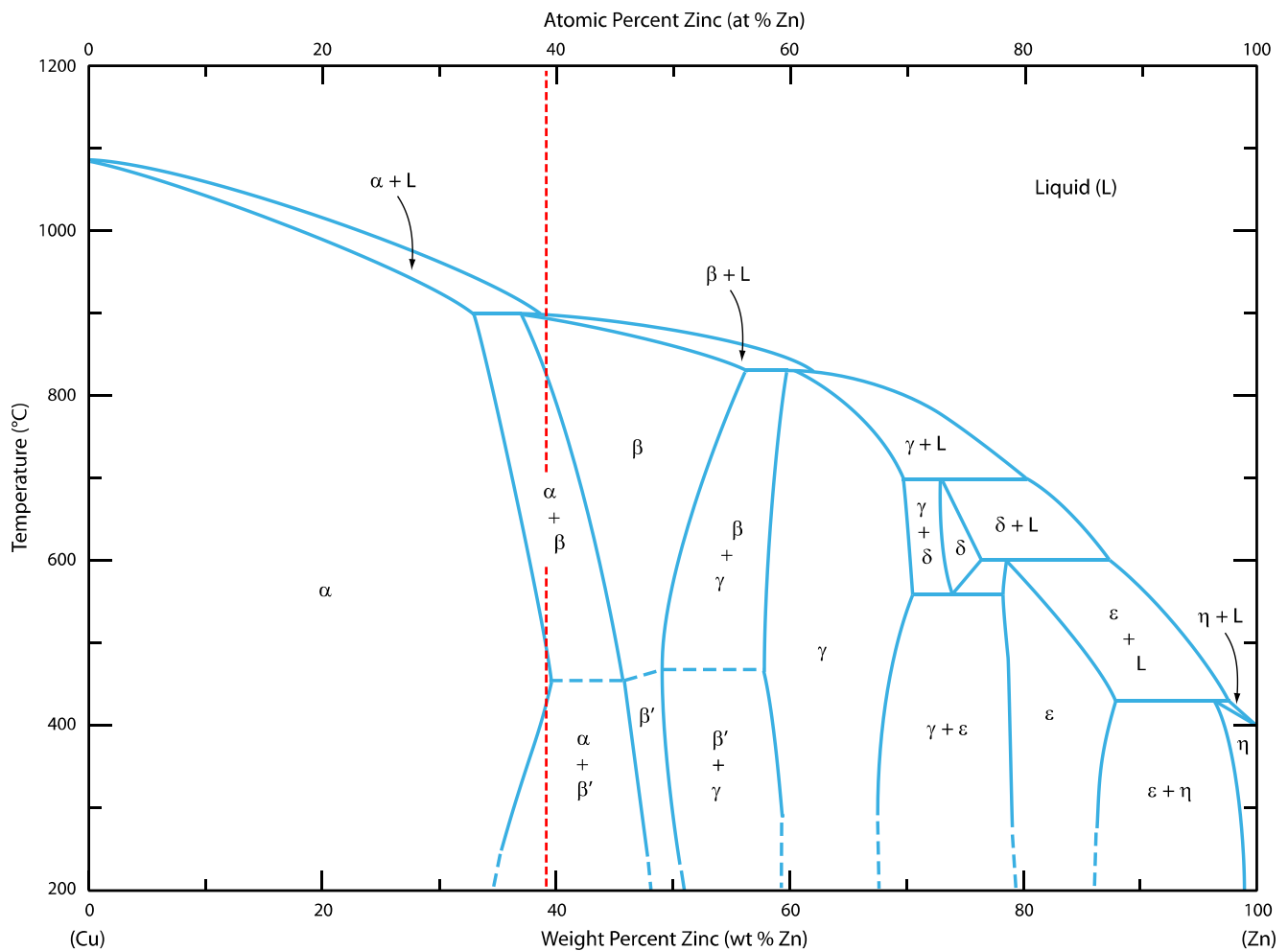


Figure 4: Copper-zinc (Cu-Zn) phase diagram. Adapted from Fig. 9.17 in “Binary Alloy Phase diagrams,” 2nd ed., Vol. 2, Massalski (Editor-in-Chief), 1990 [27].

dose implantation [24]. Finally, Cavellier completed a study on pure copper and copper alloys (brass and bronze) implanted with multi-charged nitrogen ions [25]. Several promising tribological results obtained on these materials were highlighted, related to surface hardening, especially in terms of coefficient of friction (COF) and wear rate. However, for confidentiality reasons, the associated process parameters (*i.e.*, implanted doses and energies) were not disclosed. Thus, part of his results can only be considered qualitatively.

Free machining brass

In a watch mechanism, a variety of parts are made from brass: balance wheel, bridges and bottom plate, gear train (wheels and pinions), barrel (drum and cover). Gears and drum barrel are of interest here since they have mechanical functions that require low friction and good wear resistance. To meet these requirements and ensure reliability and durability of the watch movement,

various types of lubricants are applied on these parts. Aging of lubricants is an issue and watchmakers consider lubricant-free mechanisms as their Holy Grail. Hence, one can clearly see the potential of a machinable brass with much improved tribological characteristics.

CuZn39Pb3 is one of the most commonly used brass alloys in the watchmaking industry. Lead is added to binary brass (Cu-Zn) to obtain an alloy with good machinability, a material said to be “free machining” [26]. The short metal chip breaking and the lubricating effect of lead during machining make leaded brass particularly suited for Swiss-type lathe machining (a barfed automatic turning machine known in French as “*décolleteuse*”).⁶ Figure 4 shows the phase diagram of binary brass (adapted from [27]). The vertical dashed line that is superimposed indicates the corresponding nominal concentration of Zn found in CuZn39Pb3.

The choice of CuZn39Pb3 for our scientific study was dictated, on the one hand, by the particularity of this

⁶ The European regulation REACH stipulates that Pb must be eliminated from the design of consumer goods. Currently, watchmakers are still allowed to use leaded brass for internal

components of watch timepieces which are inaccessible to consumers [Regulation No. 1907/2006 of the European Parliament and of the Council, Amendment M18].

Year	2010	2011	2012	2013	2014	2015	2016
Net sales	100.0	100.0	100.0	100.0	100.0	100.0	100.0
SG&A	10.0	10.0	10.0	10.0	10.0	10.0	10.0

Table 1. Selected components of operating leverage ratios of the 100 largest U.S. public companies (based on market capitalization) for the trailing year of 2016

and other assets than physical assets and intangible assets. In the other cases, we used the results of our research conducted in our other articles, and in some instances to compare with other intangible-related intangibles and other intangibles. In some instances, we had access to data in a public form (such as in the public domain).

The operating leverage we present in this study is a simple measure of the ratio of the change in net income to the change in net sales. We use the following equation: $OL = \frac{\Delta NI}{\Delta S}$. The ratio was derived from the data on net sales and net income from the 100 largest U.S. public companies for the trailing year of 2016. We used the following equation: $OL = \frac{\Delta NI}{\Delta S}$. The ratio was derived from the data on net sales and net income from the 100 largest U.S. public companies for the trailing year of 2016. We used the following equation: $OL = \frac{\Delta NI}{\Delta S}$.

Measurement of net income

The measure of net income we use for our study is the net income reported in the annual reports of the 100 largest U.S. public companies for the trailing year of 2016. We used the following equation: $NI = \text{Net Income}$.



Figure 2. Relationship between change in net sales and change in net income. The equation above is based on the equation with a slope of 0.85 and an intercept of 0.15.

Measurement of net sales

The measure of net sales we use for our study is the net sales reported in the annual reports of the 100 largest U.S. public companies for the trailing year of 2016. We used the following equation: $S = \text{Net Sales}$.

Net sales reported in the annual reports of the 100 largest U.S. public companies for the trailing year of 2016. We used the following equation: $S = \text{Net Sales}$. The ratio was derived from the data on net sales and net income from the 100 largest U.S. public companies for the trailing year of 2016. We used the following equation: $OL = \frac{\Delta NI}{\Delta S}$.

Measurement of operating leverage

The measure of operating leverage we use for our study is the ratio of the change in net income to the change in net sales. We used the following equation: $OL = \frac{\Delta NI}{\Delta S}$. The ratio was derived from the data on net sales and net income from the 100 largest U.S. public companies for the trailing year of 2016. We used the following equation: $OL = \frac{\Delta NI}{\Delta S}$.

The measure of operating leverage we use for our study is the ratio of the change in net income to the change in net sales. We used the following equation: $OL = \frac{\Delta NI}{\Delta S}$.

The measure of operating leverage we use for our study is the ratio of the change in net income to the change in net sales. We used the following equation: $OL = \frac{\Delta NI}{\Delta S}$.

Measurement of net sales

The measure of net sales we use for our study is the net sales reported in the annual reports of the 100 largest U.S. public companies for the trailing year of 2016. We used the following equation: $S = \text{Net Sales}$.

The measure of net sales we use for our study is the net sales reported in the annual reports of the 100 largest U.S. public companies for the trailing year of 2016. We used the following equation: $S = \text{Net Sales}$.

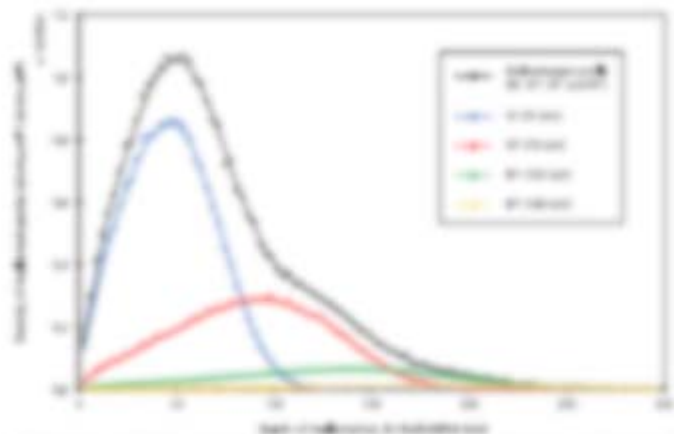


Figure 1. Evolution of the number of particles over time for each stage of the degradation process. The number of particles is plotted against time in hours for each stage.

Figure 1. It is clear that the number of particles increases over time for each stage of the degradation process. The number of particles is plotted against time in hours for each stage.

The number of particles increases over time for each stage of the degradation process. The number of particles is plotted against time in hours for each stage. The number of particles is plotted against time in hours for each stage.

The number of particles increases over time for each stage of the degradation process. The number of particles is plotted against time in hours for each stage. The number of particles is plotted against time in hours for each stage.

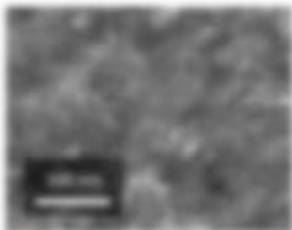
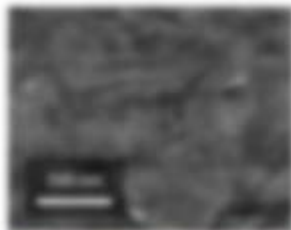


Figure 2. Two images of the surface of the degradation product. The number of particles is plotted against time in hours for each stage.

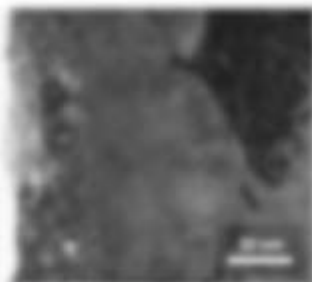
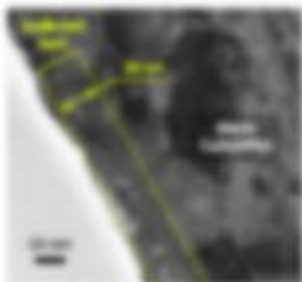


Figure 4. SEM micrographs observation of synthesized after 240 min storage temperature at 30 °C in absence of host structure. The left image is a cross-sectional view, a conventional image of about 20 μm size without any dye incorporation (left).

different stage of the sample in the presence of the synthesized host structure with a similar size in Figure 5 and in the corresponding image parts. These SEM micrographs are similar to Figure 4 in the presence of host in the same stage according to the stage of synthesis as is observed with it is shown in the corresponding image parts.

SEM analysis shows porous structure about the surface structure of ZnO. For SEM analysis, we prepared the different samples from the synthesis and prepared samples with a different size

effectively. Using various sized different ZnO particles are shown in Figure 6. The different particle sizes are similar to the different stages with porous structure in the same size stage of synthesis after synthesis of ZnO particles. For SEM image, we can conclude that different ZnO particles are obtained at 120 min and 240 min of synthesis and also ZnO particles are similar with the ZnO stage temperature in water (see Table 1).

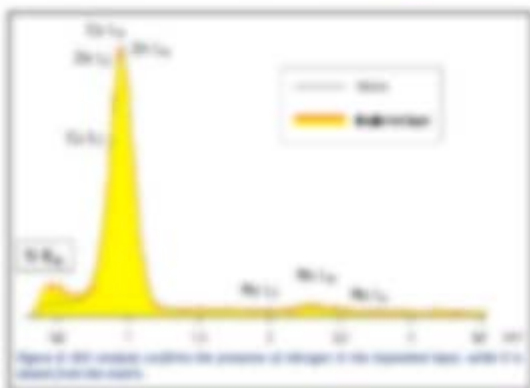


Figure 5. EDS analysis analysis the presence of stages of the synthesized host, with it is shown from the image.

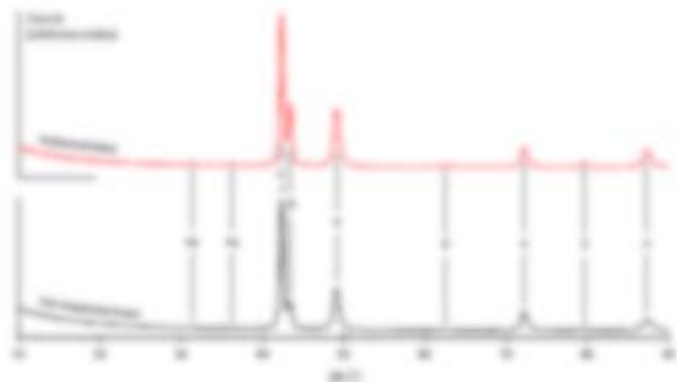


Figure 10. XRD patterns obtained from a sample of a polymer crystal. The top plot shows the experimental data, and the bottom plot shows the theoretical data. The x-axis is labeled '2θ' and the y-axis is labeled 'Intensity'.

Thermal analysis

Thermal analysis is a group of techniques used to study the changes in a material's properties as a function of temperature. The most common techniques are DSC, TGA, and TMA. DSC measures the heat flow into or out of a sample as a function of temperature. TGA measures the weight loss of a sample as a function of temperature. TMA measures the change in length of a sample as a function of temperature.

Thermal analysis is used to study the changes in a material's properties as a function of temperature. The most common techniques are DSC, TGA, and TMA. DSC measures the heat flow into or out of a sample as a function of temperature. TGA measures the weight loss of a sample as a function of temperature. TMA measures the change in length of a sample as a function of temperature.

$$T_g = \frac{1}{\alpha} \left(\frac{d\alpha}{dT} \right)_{T_g}$$

The glass transition temperature is the temperature at which the material changes from a hard, brittle state to a soft, rubbery state.

The maximum length of a polymer chain is given by the equation:

$$L_c = \frac{M_w}{M_0}$$

The weight of a polymer chain is given by the equation:

$$W = \frac{M_w}{M_0}$$

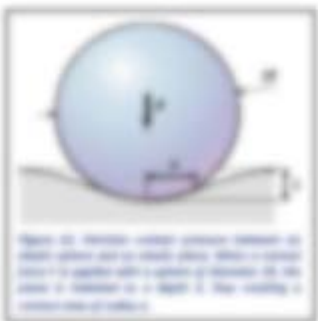


Figure 11. Schematic diagram of a spherical particle on a surface. The radius of the particle is labeled 'R', the contact radius is labeled 'r', and the height of the particle above the surface is labeled 'h'.

Year	Age group	Percentage	Year
1997	1998-2000	1997	1998-2000
1.00	1.0000	0.00	0.0000
2.00	2.0000	0.00	0.0000
3.00	3.0000	0.00	0.0000

Table 1. Percentages for each age group, by gender, for each year. Percentages are rounded down, and the values may not add up to 100% due to rounding. Percentages are shown in decimal form.

For each age group i (1997, 1998-2000), we define $x_i = 100 \times \frac{1}{n} \sum_{j=1}^n \mathbb{1}_{\{x_j = i\}}$, where $\mathbb{1}_{\{x_j = i\}}$ is the indicator function that is 1 if $x_j = i$ and 0 otherwise. We can then write the data as a vector $x = (x_1, x_2, x_3)$, where x_1 is the percentage of the population aged 1997, x_2 is the percentage of the population aged 1998-2000, and x_3 is the percentage of the population aged 1998-2000. We can then write the data as a vector $x = (x_1, x_2, x_3)$, where x_1 is the percentage of the population aged 1997, x_2 is the percentage of the population aged 1998-2000, and x_3 is the percentage of the population aged 1998-2000.

For each age group i (1997, 1998-2000), we define $y_i = 100 \times \frac{1}{n} \sum_{j=1}^n \mathbb{1}_{\{y_j = i\}}$, where $\mathbb{1}_{\{y_j = i\}}$ is the indicator function that is 1 if $y_j = i$ and 0 otherwise. We can then write the data as a vector $y = (y_1, y_2, y_3)$, where y_1 is the percentage of the population aged 1997, y_2 is the percentage of the population aged 1998-2000, and y_3 is the percentage of the population aged 1998-2000.

The change in the data can be written as a vector $z = (z_1, z_2, z_3)$, where z_1 is the change in the percentage of the population aged 1997, z_2 is the change in the percentage of the population aged 1998-2000, and z_3 is the change in the percentage of the population aged 1998-2000.

- The data is represented by the vector x .
- The data is represented by the vector y .
- The data is represented by the vector z .
- The data is represented by the vector x .

For the data, we can write the vector x as $x = (x_1, x_2, x_3)$, where x_1 is the percentage of the population aged 1997, x_2 is the percentage of the population aged 1998-2000, and x_3 is the percentage of the population aged 1998-2000. We can then write the data as a vector $x = (x_1, x_2, x_3)$, where x_1 is the percentage of the population aged 1997, x_2 is the percentage of the population aged 1998-2000, and x_3 is the percentage of the population aged 1998-2000.

We can then write the data as a vector $x = (x_1, x_2, x_3)$, where x_1 is the percentage of the population aged 1997, x_2 is the percentage of the population aged 1998-2000, and x_3 is the percentage of the population aged 1998-2000. We can then write the data as a vector $x = (x_1, x_2, x_3)$, where x_1 is the percentage of the population aged 1997, x_2 is the percentage of the population aged 1998-2000, and x_3 is the percentage of the population aged 1998-2000.

For each age group i (1997, 1998-2000), we define $x_i = 100 \times \frac{1}{n} \sum_{j=1}^n \mathbb{1}_{\{x_j = i\}}$, where $\mathbb{1}_{\{x_j = i\}}$ is the indicator function that is 1 if $x_j = i$ and 0 otherwise. We can then write the data as a vector $x = (x_1, x_2, x_3)$, where x_1 is the percentage of the population aged 1997, x_2 is the percentage of the population aged 1998-2000, and x_3 is the percentage of the population aged 1998-2000. We can then write the data as a vector $x = (x_1, x_2, x_3)$, where x_1 is the percentage of the population aged 1997, x_2 is the percentage of the population aged 1998-2000, and x_3 is the percentage of the population aged 1998-2000.

For each age group i (1997, 1998-2000), we define $y_i = 100 \times \frac{1}{n} \sum_{j=1}^n \mathbb{1}_{\{y_j = i\}}$, where $\mathbb{1}_{\{y_j = i\}}$ is the indicator function that is 1 if $y_j = i$ and 0 otherwise. We can then write the data as a vector $y = (y_1, y_2, y_3)$, where y_1 is the percentage of the population aged 1997, y_2 is the percentage of the population aged 1998-2000, and y_3 is the percentage of the population aged 1998-2000. We can then write the data as a vector $y = (y_1, y_2, y_3)$, where y_1 is the percentage of the population aged 1997, y_2 is the percentage of the population aged 1998-2000, and y_3 is the percentage of the population aged 1998-2000.

The change in the data can be written as a vector $z = (z_1, z_2, z_3)$, where z_1 is the change in the percentage of the population aged 1997, z_2 is the change in the percentage of the population aged 1998-2000, and z_3 is the change in the percentage of the population aged 1998-2000. We can then write the data as a vector $z = (z_1, z_2, z_3)$, where z_1 is the change in the percentage of the population aged 1997, z_2 is the change in the percentage of the population aged 1998-2000, and z_3 is the change in the percentage of the population aged 1998-2000.

$$z = \begin{pmatrix} z_1 \\ z_2 \\ z_3 \end{pmatrix}$$

- The data is represented by the vector x .
- The data is represented by the vector y .
- The data is represented by the vector z .
- The data is represented by the vector x .

For the data, we can write the vector x as $x = (x_1, x_2, x_3)$, where x_1 is the percentage of the population aged 1997, x_2 is the percentage of the population aged 1998-2000, and x_3 is the percentage of the population aged 1998-2000. We can then write the data as a vector $x = (x_1, x_2, x_3)$, where x_1 is the percentage of the population aged 1997, x_2 is the percentage of the population aged 1998-2000, and x_3 is the percentage of the population aged 1998-2000.

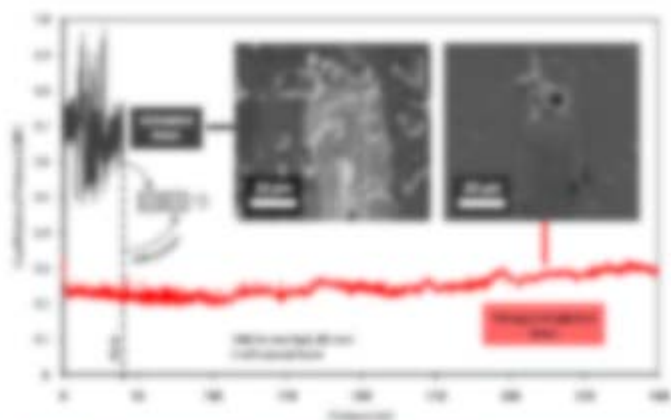


Figure 19. Evolution of the average diameter of a cell over time. The cell is initially at a diameter of approximately 40 micrometers. At 120 minutes, the cell is at a diameter of approximately 50 micrometers. The inset images show the cell at different stages of its growth. The inset image at 0 minutes shows a large, irregularly shaped cell. The inset image at 120 minutes shows a smaller, more rounded cell.

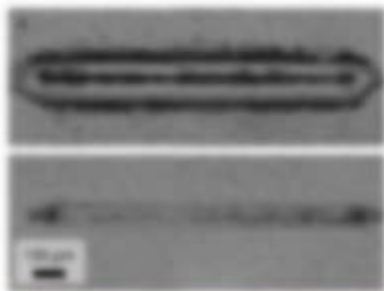


Figure 20. Comparison of the diameter of a cell over time. The cell is initially at a diameter of approximately 40 micrometers. At 120 minutes, the cell is at a diameter of approximately 50 micrometers. The inset images show the cell at different stages of its growth. The inset image at 0 minutes shows a large, irregularly shaped cell. The inset image at 120 minutes shows a smaller, more rounded cell.

Discussion and outlook

This study has shown that it is possible to create a cell in a petri dish. The cell is initially at a diameter of approximately 40 micrometers. At 120 minutes, the cell is at a diameter of approximately 50 micrometers. The inset images show the cell at different stages of its growth. The inset image at 0 minutes shows a large, irregularly shaped cell. The inset image at 120 minutes shows a smaller, more rounded cell. The cell is initially at a diameter of approximately 40 micrometers. At 120 minutes, the cell is at a diameter of approximately 50 micrometers. The inset images show the cell at different stages of its growth. The inset image at 0 minutes shows a large, irregularly shaped cell. The inset image at 120 minutes shows a smaller, more rounded cell.

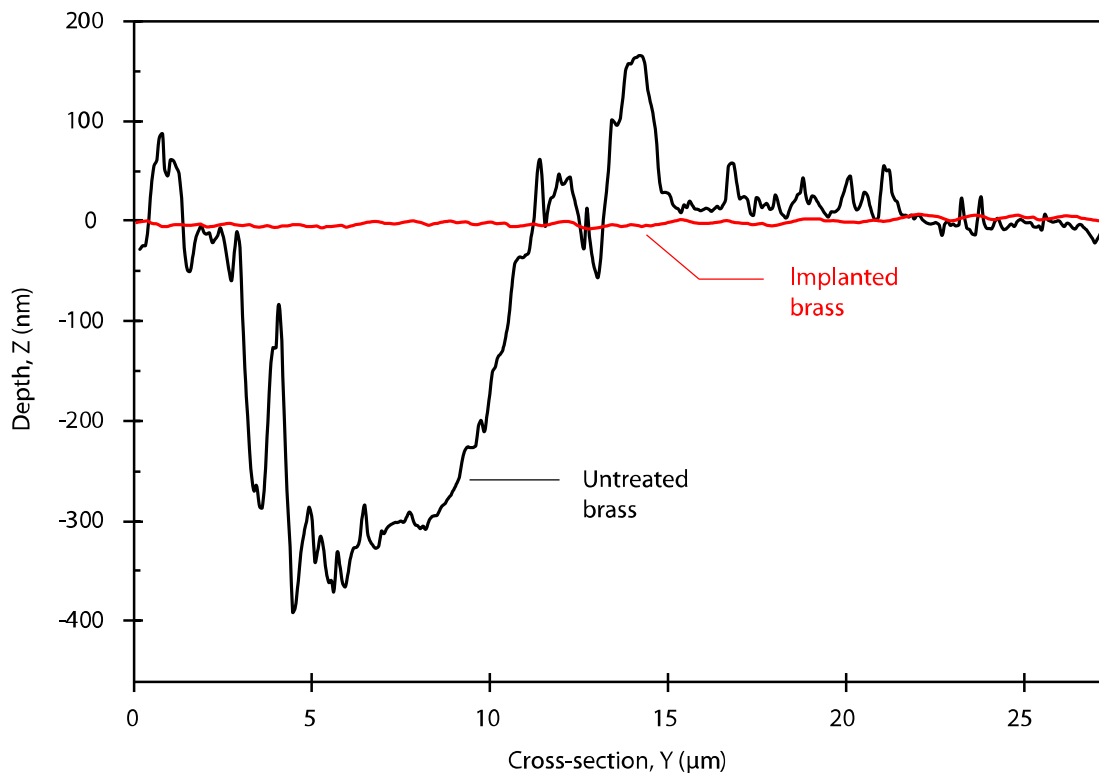


Figure 14: AFM measurements of the traces shown in Figure 13. Note the difference in scales between Y cross-section (μm) and Z depth (nm). The wear rate of brass could be reduced by two orders of magnitude thanks to ion implantation.

[21]. These results pave the way for the use of nitrogen-implanted brass parts in applications where lifetime and mechanical load usually proscribe untreated brass.

We conclude this white paper by highlighting that ion implantation is a high potential technology that can be used for many other materials, and for applications that are not limited to tribological enhancement. We are working hand in hand with watchmakers and clients from other industrial sectors to develop the technology and provide dedicated processes tailored to their specific needs. ■

Acknowledgment

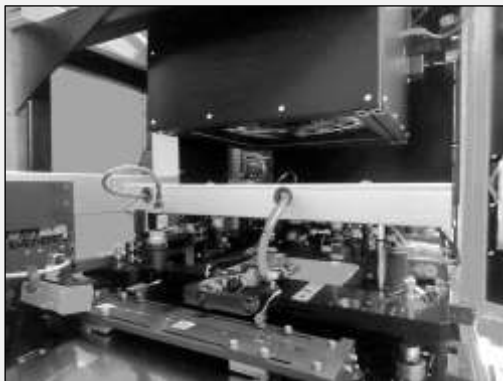
This research was completed in collaboration with the CSEM (division "Materials Science and Component Reliability") through funding No. 25480.1 PFNM-NM granted by the Commission for Technology and Innovation (CTI, Switzerland), now known as Innosuisse.

References

- [1] W. Shockley, "Forming semiconductive devices by ionic bombardment". Patent US2787564, 1954.
- [2] L. Rubin and J. Poate, "Ion implantation in silicon technology," *The Industrial Physicist*, vol. 9, no. 3, pp. 12-15, 2003.
- [3] J. F. Ziegler, M. D. Ziegler and J. P. Biersack, "SRIM – The stopping and range of ions in matter," *Nuclear Instruments and Methods in Physics Research Section B: Beam Interactions with Materials and Atoms*, vol. 268, no. 11-12, pp. 1818-1823, 2010.
- [4] "SRIM – The Stopping and Range of Ions in Matter," [Online]. Available: <http://www.srim.org>.
- [5] N. Angert, "Ion sources," in *CAS – CERN Accelerator School: Fifth General Accelerator Physics Course*, CERN, Ed., Jyväskylä (Finland), September 1992, pp. 619-642.
- [6] R. Geller, "ECRIS: The electron cyclotron resonance ion sources," *Annual Review of Nuclear and Particle Science*, vol. 40, pp. 15-43, 1990.
- [7] R. Geller, "ECRIS: The electron cyclotron resonance ion sources – (status)," in *Atomic Physics of Highly Charged Ions*, E. Salzborn, P. H. Mokler and A. Müller, Eds., Berlin, Heidelberg, Springer, 1991, pp. S117-S121.
- [8] G. J. Brakenhoff and A. Goede, "A warm quiescent plasma in a minimum B-field obtained with permanent magnets," *Plasma Physics*, vol. 12, no. 10, pp. 815-817, 1970.
- [9] K. Halbach, "Design of permanent multipole magnets with oriented rare earth cobalt material," *Nuclear Instruments and Methods*, vol. 169, no. 1, pp. 1-10, 1980.
- [10] M. Schlapp, R. Trassl, E. Salzborn, R. W. McCullough, T. K. McLaughlin and H. B. Gilbody, "An ultra compact 10 GHz electron-cyclotron-resonance ion source (ECRIS) for multiply charged ions production," *Nuclear Instruments and Methods in Physics Research Section B: Beam*

- Interactions with Materials and Atoms*, vol. 98, pp. 525-527, 1995.
- [11] P. Sortais, C. Bieth and S. Kantas, "Dispositif pour la production d'ions de charges positives variables et à résonance cyclotronique". Patent EP1272015A1, 2003.
- [12] L. A. Giannuzzi, B. I. Prenitzer and B. W. Kempshall, "Ion - Solid Interactions," in *Introduction to Focused Ion Beams: Instrumentation, Theory, Techniques and Practice*, L. A. Giannuzzi and F. A. Stevie, Eds., Boston, MA: Springer US, 2005, pp. 13-52.
- [13] L. A. Larson, J. M. Williams and M. I. Current, "Ion implantation for semiconductor doping and materials modification," *Reviews of Accelerator Science and Technology*, vol. 4, no. 1, pp. 11-40, 2011.
- [14] P. Budzyński, P. Tarkowski, E. Jartych and A. P. Kobzev, "Evolution of mechanical properties in tool steel implanted with high energy nitrogen ions," *Vacuum*, vol. 63, no. 4, pp. 737-742, 2001.
- [15] P. Budzynski, "Long-range effect in nitrogen ion-implanted AISI 316L stainless steel," *Nuclear Instruments and Methods in Physics Research Section B: Beam Interactions with Materials and Atoms*, vol. 342, pp. 1-6, 2015.
- [16] P. Budzyński, M. Kamiński, A. Drożdźiel and M. Wiertel, "Long-range effect of ion implantation of Raex and Hardox steels," *IOP Conference Series: Materials Science and Engineering*, vol. 148, no. 1, pp. 1-8 (012045), 2016.
- [17] R. J. Rodriguez, A. Sanz, A. Medrano and J. Garcia -Lorente, "Tribological properties of ion implanted Aluminum alloys," *Vacuum*, vol. 52, no. 1-2, pp. 187-192, 1999.
- [18] E. Hug, S. Thibault, D. Chateigner and L. Maunoury, "Nitriding aluminum alloys by N-multicharged ions implantation: Correlation between surface strengthening and microstructure modifications," *Surface and Coatings Technology*, vol. 206, no. 24, pp. 5028-5035, 2012.
- [19] P. Budzynski and J. Sielanko, "Long-range effect in ion-implanted titanium alloys," *Acta Physica Polonica A*, vol. 128, pp. 841-844, 2015.
- [20] K. K. Shih, "Effect of nitrogen ion implantation on impact wear," *Wear*, vol. 105, no. 4, pp. 341-347, 1985.
- [21] G. Dearnaley, "Adhesive and abrasive wear mechanisms in ion implanted metals," *Nuclear Instruments and Methods in Physics Research Section B: Beam Interactions with Materials and Atoms*, Vols. 7-8, pp. 158-165, 1985.
- [22] A. H. Sari, M. K. Salem and A. Shoorche, "Effect of nitrogen ion implantation in copper," *Journal of Fusion Energy*, vol. 30, no. 4, pp. 323-327, 2011.
- [23] S. Y. Zharkov, V. P. Sergeev, A. R. Sungatulin and M. P. Kalashnikov, "Wear of nitrogen ion implanted copper with tribological Cu-Mo-S coatings," *AIP Conference Proceedings*, vol. 1909, pp. 1-4 (020238), 2017.
- [24] V. Sergeev, A. R. Sungatulin, M. P. Kalashnikov, O. V. Sergeev and S. Y. Zharkov, "Microstructure and wear resistance of surface layer of copper modified by N+ ion high fluencies implantation," *Advanced Materials Research*, vol. 1085, pp. 201-204, 2015.
- [25] M. Cavellier, "Study of nitrogen ion implantation effects on pure magnesium, pure copper and copper alloys properties," PhD thesis, INSA, Rennes (France), 2012.
- [26] Copper Development Association (CDA), "Equilibrium diagrams – Selected copper alloy diagrams illustrating the major types of phase transformation," CDA Publication No. 94, 1992. [Online]. Available: <http://copperalliance.org.uk>.
- [27] T. B. Massalski, H. Okamoto, P. R. Subramanian and L. Kacprzak, Eds., "Binary Alloy Phase diagrams," 2nd ed., ASM International, 1990.
- [28] R. Budynas and K. Nisbett, *Shigley's Mechanical Engineering Design*, 9th ed., McGraw-Hill Series in Mechanical Engineering, 2012.

Creative engineering and manufacturing • Our engineering team is accustomed to developing products according to client's needs. In-house machining and assembling facilities shorten the time from concept to finished products.



Customized UV-LED exposure system installed on a roll-to-roll machine

Visit our website to have an insight into our other products and activities. Contact us for further technical information and to obtain a quotation.



Double image microscope



A model of wafer chuck